International Conference on Greenhouse Gas Technologies (GHGT-12)

Models for CO$_2$ injection with coupled thermal processes

Bawfeh K. Kometa[a,*], Sarah E. Gasda[b], Ivar Aavatsmark[b]

^{a}Mathematics Institute, University of Bergen, Allegatan 41, 5020, Bergen, Norway
^{b}Centre for Integrated Pertroleum Research, Uni-Research, Allegatan 41, 5020, Bergen, Norway

Abstract

Large-scale models of carbon dioxide (CO$_2$) storage in geological formations must capture the relevant physical, chemical and thermodynamic processes that affect the migration and ultimate fate of injected CO$_2$. These processes should be modeled over the appropriate length and time scales. Some important mechanisms include convection- driven dissolution, caprock roughness, and local capillary effects, all of which can impact the direction and speed of the plume as well as long-term trapping efficiency. In addition, CO$_2$ can be injected at a different temperature than reservoir conditions, leading to significant density variation within the plume over space and time. This impacts buoyancy and migration patterns, which becomes particularly important for injection sites with temperature and pressure conditions near the critical point. Therefore, coupling thermal processes with fluid flow should be considered in order to correctly capture plume migration and trapping within the reservoir. This study focuses on compositional non- isothermal flow using 3D and vertically upscaled models. The model concept is demonstrated on simple systems. In addition, we explore CO$_2$ thermodynamic models for reliable prediction of density under different injection pressures, temperatures and composition.

1. Introduction

Understanding the non-isothermal processes involved in large-scale CO$_2$ storage in porous media has been an issue of interest in recent years; see e.g., the work of [6, 3, 4] and references therein. This study focuses on compositional non-isothermal flow using 3D. The model concept is demonstrated on simple systems. In addition, we explore CO$_2$ thermodynamic models for reliable prediction of density under different injection pressures, temperatures and composition. To demonstrate the thermal effects on CO$_2$ injection models, simulation results obtained with various optimized equations of state for CO$_2$ are compared. For the sake of simplicity, we focus on two-phase two-component immiscible (water-CO$_2$) systems described by a compositional flow model. The verified

concepts can easily be extended to include miscible three-phase systems with salt, hydrocarbon or natural gas impurities.

The rest of the paper is organized as follows: section 2 contains a brief description of the compositional flow model considered; section 3 contains a brief description of Aavatsmark's improvement on the generalized cubic equation of state [1]; in section 4 some simulation examples are described; in section 5 we make a comparison of the different equations of state (EOS) in the considered numerical simulations.

Nomenclature

EOS   Equation(s) of state
SW   Span-Wagner
PR   Peng-Robbinson
SRK   Soave-Redlich-Kwong
CO_2 Carbon dioxide
G   Optimized generalized cubic equation of state

---

2. Compositional flow model

We consider the mathematical model for multi-phase, multi-component systems described in detail by [9], namely:

$$\frac{1}{V}\frac{\partial N^v}{\partial t} + \boldsymbol{\nabla} \cdot \left(\sum_{\alpha} \varrho_\alpha (\mathbf{u}_\alpha X_\alpha^v - S_\alpha \mathbf{D}_\alpha^v \boldsymbol{\nabla} X_\alpha^v) \right) = q^v \tag{1}$$

$$(1-\phi)\rho_s \frac{\partial h_s}{\partial T}\frac{\partial T}{\partial t} + \frac{\partial}{\partial t}\left(\phi \sum_{\alpha \neq s} \rho_\alpha S_\alpha u_\alpha \right) + \boldsymbol{\nabla} \cdot \left(\sum_{\alpha} (\rho_\alpha \mathbf{u}_\alpha h_\alpha - \boldsymbol{\kappa}_\alpha \boldsymbol{\nabla} T) \right) = q^e \tag{2}$$

$$\frac{R(t)}{\Delta t} + \frac{\partial R}{\partial p_w}\frac{\partial p_w}{\partial t} + \frac{\partial R}{\partial T}\frac{\partial T}{\partial t} + \sum_{\alpha}\frac{\partial R}{\partial N^v}\frac{\partial N^v}{\partial t} = 0 \tag{3}$$

where $v = 1, \cdots, n_c$ and $\alpha = w, o, g$ (water, NAPL/oil, gas) denote the component and phase indices respectively. The subscript s represents the solid phase. Equation (1) describes the mass balance for each component; (2) is the energy balance equation; (3) is added to ensure that the pore volume (ϕV) is fully occupied by the fluid phases, at every advancement in time from t to $t + \Delta t$. This is achieved via linearization of the residual volume $R(t + \Delta t)$ about t. For each phase the corresponding Darcy flux is denoted by $\mathbf{u}_\alpha$. The model is defined in terms of primary variables p_w (water-phase pressure), and T (temperature), N^v (number of moles of each component). Secondary variables include the porosity (ϕ), phase volume (V_α), residual volume ($R := \phi V - \sum_\alpha V_\alpha$) phase saturation ($S_\alpha$), phase mass density ($\rho_\alpha$), phase molar density ($\varrho_\alpha$), phase enthalpy ($h_\alpha$), phase internal energy (u_α), and the composition of each component in each phase (X_α^v). Matrix coefficients $\mathbf{D}_\alpha^v$ and $\boldsymbol{\kappa}_\alpha$ denote the phase diffusion and Fourier conductivity tensors respectively. Suitable outlet/inlet source terms such as the injection rates (q^v) and external energy fluxes (q^e) are also taken into account.

For a closed description of the system suitable thermodynamic models are required to determine phase state variables $\varrho_\alpha, \rho_\alpha, u_\alpha, h_\alpha, V_\alpha$. The model by [11] happens to be one of the most accurate model for representing CO_2 thermodynamic properties. However, cubic equations of state (EOS) appear to be the most used in commercial simulation tools such as ECLIPSE [10], GEM [7] etc. They are easier to implement directly in large-scale simulations than the Span-Wagner (SW) model.

The simulation is run using RS/Athena1. RS/Athena implements a black-oil formulation of the compositional flow model, in which (1) and (2) are solved implicitly (in time) for the pressure pw, and temperature T, using a sequential splitting approach. Meanwhile (1) are solved explicitly for the N^v (hence the saturations), like for an IMPES2 method. The spatial discretization method is the standard finite volume method, with two-point or multi-point flux approximations (TPFA/MPFA). RS/Athena also provides the option for direct implementation of the cubic EOS, in which phase equilibrium is achieved via a balance of phase fugacities.

3. Generalized cubic equation of state

Various modifications have been made to improve the accuracy of the cubic EOS. One such improvement, recently presented by [1] (see also [2]), is briefly discussed in this section. A generalized cubic EOS may be written in the form

$$p = \frac{\bar{R}T}{v - b} - \frac{a \cdot \hat{a}(T)}{(v - \delta_1 b)(v - \delta_2 b)}$$

(4)

where $\delta_1 < \delta_2 < 1$. Special cases of this cubic EOS are the PR equation with $\delta_1 = -(\sqrt{2} + 1)$ and $\delta_2 = \sqrt{2} - 1$ and the SRK equation with $\delta_1 = -1$ and $\delta_2 = 0$. Also the van der Waals equation is a special case of this form with $\delta_1 = \delta_2 = 0$, although it does not satisfy the required inequality for δ_1 and δ_2. Following Soave, the function $\hat{a}(T)$ should have the form

$$\hat{a}(T) = \left[1 + \kappa \left(1 - \sqrt{T/T_c}\right)\right]^2,$$

where T_c is the critical temperature and κ is a parameter to be determined. The constants a and b are defined by

$$a = \Omega_a \frac{\bar{R}^2 T_c^2}{p_c}, \qquad b = \Omega_b \frac{\bar{R}T_c}{p_c}$$

(5)

where pc is the critical pressure, and $\bar{R}$ is the universal molar gas constant. Values of the constants Ω_a and Ω_b are determined by fitting the right behaviour at the critical point.

The parameters δ_1, δ_2 and κ may be chosen to give an equation of state with an improved accuracy for a given substance in a given region of temperature and pressure. For CO_2 for example, comparing the cubic equation of state to the SW equation [11], an optimal choice of δ_1, δ_2 and κ which gives the least root-mean-square (RMS) error in the density may be found.

As an example, CO_2 in the temperature-pressure region 300–320 K and 8–10 MPa is considered. This is approximately the temperature-pressure region of the Sleipner field. The choice which gives the least RMS error of the density is given by

$$\delta_1 = -3.19, \qquad \delta_2 = 0.082, \qquad \kappa = 0.68.$$

In Fig. 1 the densities of the SW equation the PR equation and the new cubic EOS are compared for the given temperature-pressure region. In Fig. 2 the density deviations (from the SW densities) of the PR equation and the new cubic EOS are compared. The RMS error for these two cubic EOS are 51.6 kg/m3 and 17.6 kg/m3, respectively. Hence the optimal choice of parameters for CO_2 in the temperature-pressure region of the Sleipner field yields an error in the density which is approximately 3 times smaller than the error when using the PR equation.

In this study we show that different formulations of the cubic EOS may affect numerical simulations of the flow and storage of injected CO_2 significantly. We demonstrated with two simulation examples.

————

[1] This is an in-house reservoir simulation tool developed by the Centre for Integrated Petroleum Research (CIPR), Bergen, Norway
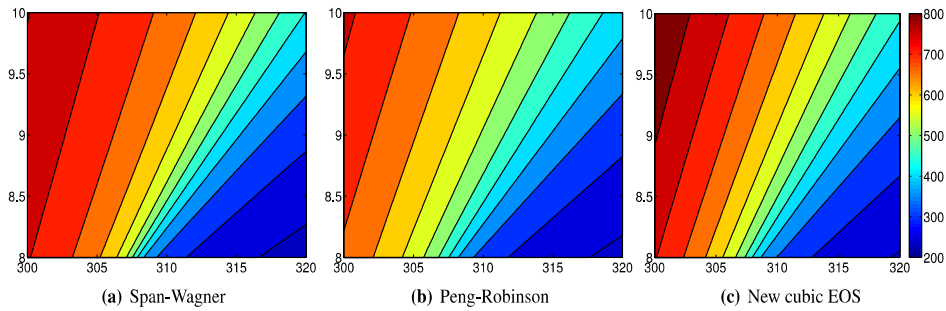[2] Implicit Pressure, Explicit Saturation

Fig. 1. Isochores [kg/m^3]. Pressure [MPa] (vertical axis), Temperature [K] (horizontal axis).
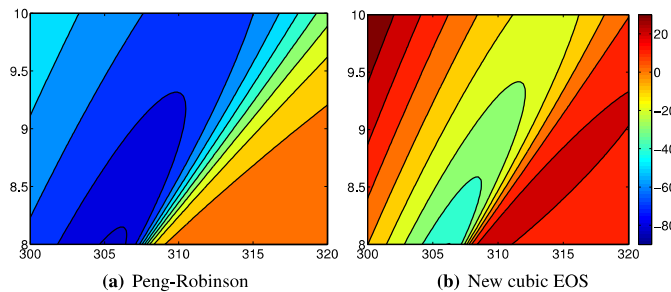

Fig. 2. Deviation [kg/m^3]. Pressure [MPa] (vertical axis), Temperature [K] (horizontal axis).

4. Numerical simulations

4.1. Simulation 1

In this simulation, following [3], we consider a rectangular domain Ω of dimension 500 m by 500 m (in the xz-plane) situated at a depth of 500 m below the surface (see Fig. 3). Ω is initially fully saturated with water at reservoir temperature of 37℃ and a pressure of about 5 MPa. Warm CO_2 (temperature 37℃) is injected at a depth of about 900 m, at a constant rate of 1.25 kg/s, over a period of 30 days. The specified boundary conditions are no-flow Neumann at the left and top, except at the injection region on the left (approximately 80 - 120 m from the bottom). Dirichlet conditions consistent with the initial data are imposed at the right and bottom. Hydrostatic pressure initial conditions are imposed throughout the domain. The SW equation of state has been used to approximate the CO_2 thermodynamic properties. For the CO_2 dynamic viscosities, the correlation proposed by [8] is applied. The spatial discretization is done so that the injection rate per unit cross-section area is 0.02 kg/(m^2s). A complete description of the reservoir properties, fluid properties and rock-fluid parameters is given in Tables A.3 and A.4 of the Appendix.

The results are shown in Fig. 5. In this short-term injection process, we observe that the CO_2 cools off significantly as it expands from the injection region, leading to large densities that decreases upwards in regions of lower pressure. Buoyancy leads to accumulation of CO_2 at the top of the reservoir. Fig. 5(d) shows CO_2 phase diagrams with temperature-pressure variation along the vertical line (L_{vert}) on the left boundary, and the horizontal line (L_{hori}) at the injection depth. These transects are used for later comparison of EOS formulations. It should be

noted that the vertical transect passes quite close to the critical point of CO_2 near z = −680 m, which is where we expect the largest deviation of the standard cubic EOS formations from the SW data.
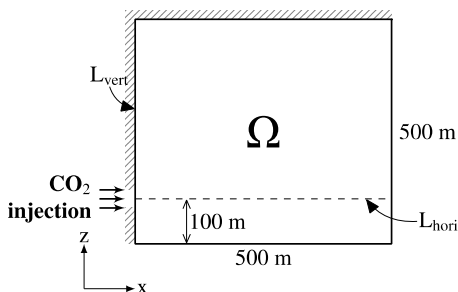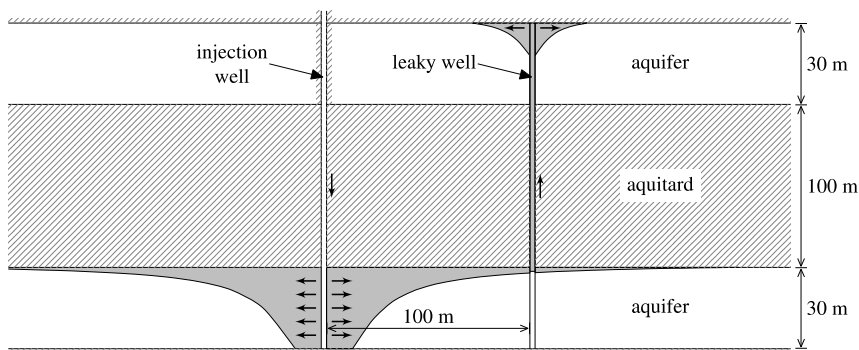

Fig. 3. The 2D reservoir domain of Simulation 1.

Fig. 4. Leakage scenario in 3D reservoir.

4.2. Simulation 2

Here we consider the benchmark problem by [5], modeling a CO_2 leakage scenario. The domain consists of a 3D cuboid, 1000 m by 1000 m by 160 m, situated at a depth of 640 m below the surface of the earth. It is comprised of two aquifers (each 30 m thick) seperated by an aquitard of thickness 100 m (see Fig. 4). CO_2 is injected through a vertical well into the lower aquifer at constant rate of 8.87 kg/s, over a continuous duration of 2000 days. At the centre of the domain is an abandoned vertical well, located at a distance of 100 m away from the injection well. After some duration of the injection, the CO_2 begins to leak into the upper aquifer via the abandoned well. The (homogeneous) porous media are initially fully saturated with water, and have a constant geothermal gradient of 0.03 K/m. The initial temperature and pressure at the bottom (800 m deep) are 34 °C and 8.499×10^7 Pa respectively. Hydrostatic pressure initial conditions are applied in the entire domain. The temperature of the injected CO_2 is 33.6°C). On the lateral boundaries are imposed constant Dirichlet conditions, equal to the initial conditions, while no- flow Neumann condtions are imposed on all other boundaries. The leaky well is modeled as a porous medium with a higher permeability than the rest of the formation. For a complete description of the porous media properties, the rock properties and rock-fluid parameters, we refer the reader to [5]. In this example we have

considered isothermal flow conditions. Again we assume negligible mutual miscibilities of the CO_2 and water phases, and the thermodynamic properties of pure water are used for the water phase.
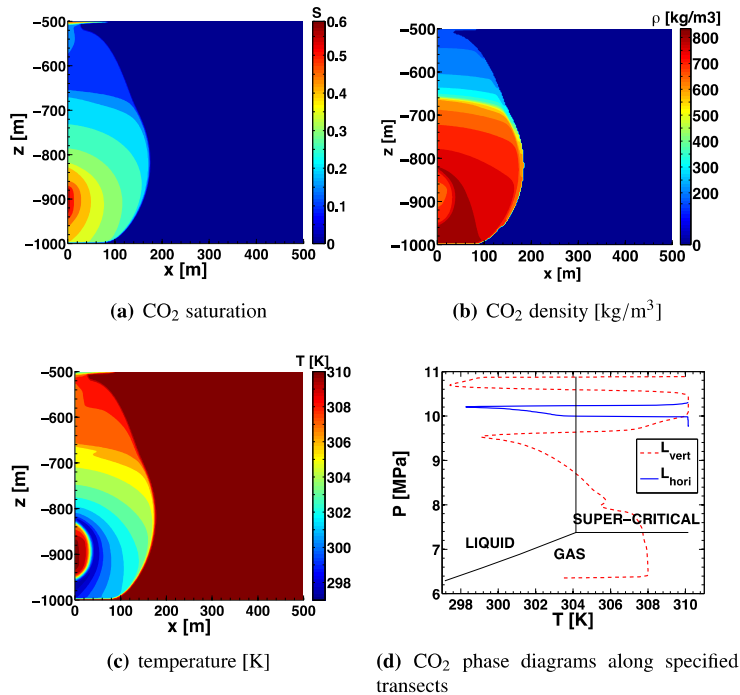

(a) CO_2 saturation

(b) CO_2 density [kg/m³]

(c) temperature [K]

(d) CO_2 phase diagrams along specified transects

Fig. 5. Simulation results after 30 days of injection.

5. Comparison of cubic EOS with SW

In this section we consider different cubic EOS for CO_2, and compare their performances in the numerical simulations described in section 4. The comparisons are also made against corresponding results obtained with the SW data, as a reliable and accurate benchmark for CO_2 thermodynamic properties.

5.1. From Simulation 1

In Fig. 6 we show the differences in the saturation and density along the vertical line L_{vert} and along the horizontal line L_{hori} (cf. Fig. 3), for a series of simulations done with a selected number of EOS reported in Table 1. For the system described in Simulation 1, parameters of the generalized EOS have been optimally chosen for CO_2 in the temperature-pressure region 297–310 K and 5–11 MPa respectively. Also reported in Table 1 are values of the constants Ω_a, Ω_b defined in (5). The last column of the table shows the root-mean-square deviation (RMSD) in CO_2 densities from the SW data, over the pressure and temperature ranges 5–11 MPa and 297–310 K respectively.

We observe a significant difference in the CO_2 densities in the vertical direction L_{vert} (cf. Figure 6(d)). At depths below 680 m (approximately), the EOS formulations by PR and SRK appear to under-estimate the densities, when

compared with SW. On the other hand, vtPR tends to over-estimate the densities. The EOS formulation by Aavatsmark (G) shows a much better agreement with the SW data, as one would expect from the RMSD values reported in Table 1. The difference in densities also accounts for the additional buoyancy effect observed with PR and SRK (higher CO_2 saturation seen at the reservoir top, in Fig. 6(b)), and the reduced buoyancy effect with vtPR. Similar observations are seen along the horizontal direction L_{hori} (cf. Figure 6(c)). As shown earlier in Figure 5(d), along the lines L_{vert} and L_{hori}, the CO_2 thermodynamic state approaches the critical and supercritical regions respectively. The standard cubic EOS (PR, SRK, vtPR) give worse approximations in these regions. We observe corresponding differences when comparing the temperatures.

Table 1. Parameters used for the cubic equations of states

EOS		δ_1	δ_2	κ	Ω_a	Ω_b	RMSD[kg/m^3]
Peng-Robinson	PR	$-1-\sqrt{2}$	$-1+\sqrt{2}$	0.7056	0.4572	0.0778	49.1
volume-translated PR	vtPR	-4.9009	-0.0124	0.7056	0.4572	0.0450	77.9
Soave-Redlich-Kwong	SRK	-1	0	0.8263	0.4275	0.0866	100.3
Aavatsmark	G	-3.7236	0.8624	0.2716	0.5515	0.0947	20.5

5.2. From Simulation 2

The main outcome of *Simulation 2* is the leakage rate, defined in [5] as the CO_2 mass flow rate across the centre of the leaky well as a function of time. This is reported as a percentage fraction of the injection. Shown in Fig. 7 are the leakage rates obtained with the different cubic EOS (cf. Table 1) and the SW data. Again we observe significant discrepancies in the results from the different cubic EOS and the SW data. More importantly we notice that these differences are consistent with the observations made in Simulation 1. Therefore similar conclusions about the buoyancy effects apply here as well. For further detail on the differences observed in Fig. 7, we report in Table 2 the maximum leakage rate, the time at which this maximum is attained, the leakage rate at the end of 2000 days, and time of arrival of the CO_2 plume at the leaky well. Comparing the results, we see a better match between the SW data and the generalized cubic EOS (G), than with the other cubic EOS. We remark that the same simulation was carried out in [5] by different research groups, using different simulation tools based on different numerical discretization methods. A wide spectrum of discrepancies was observed when comparing their results (cf. Fig. 7(b)). We assert that one reason for those discrepancies would be the differences in the thermodynamic (PVT) formulations applied in the different simulation tools, apart from differences in the spatial and temporal accuracies of the discretization methods used. This assertion is justifiable from our results.

Table 2. Results of simulation 2. Comparing simulation results for the different EOS.

EOS	abbrev.	Maximum leakage rate [%]	Time at maximum [days]	Leakage rate at 2000 days [%]	Arrival time [days]
Peng-Robinson	PR	0.1131	461	0.0879	38
volume-translated PR	vtPR	0.0816	805	0.0711	57
Soave-Redlich-Kwong	SRK	0.1279	351	0.0954	31
Aavatsmark	G	0.1027	518	0.0815	41
Span-Wagner	SW	0.1034	505	0.0805	38

(a) CO₂ saturation along L_hori

(b) CO₂ saturation along L_vert

(c) CO₂ density [kg/m³] along L_hori

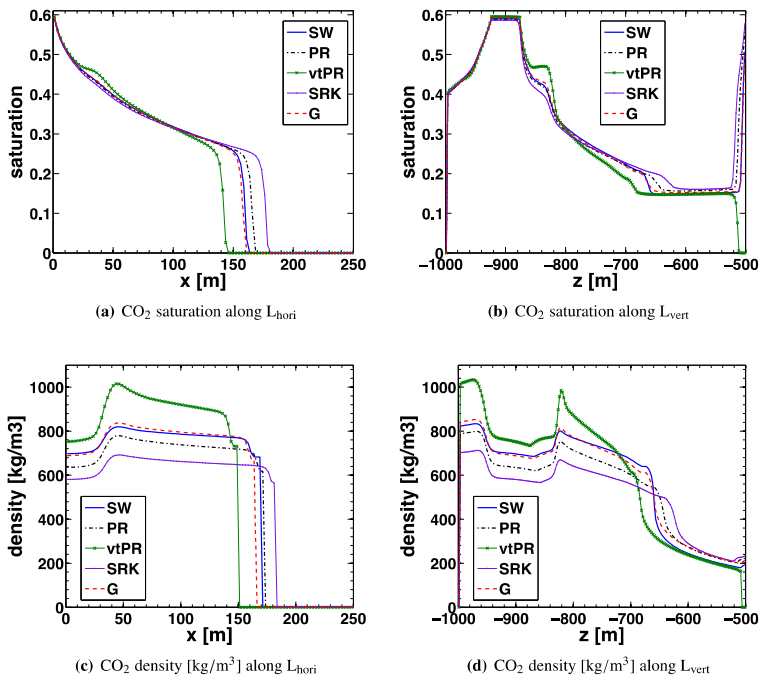**(d)** CO₂ density [kg/m³] along L_vert

Fig. 6. Simulation results after 30 days of injection: Comparing the different cubic EOS against SW.
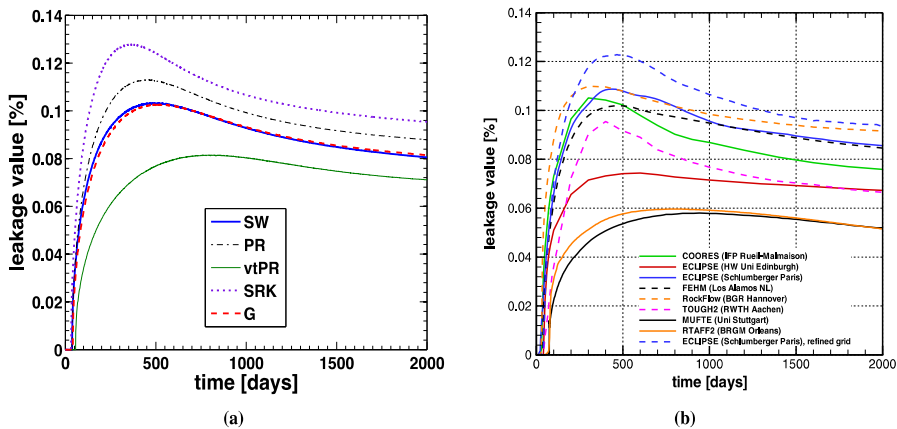

(a)

(b)

Fig. 7. (a) Results of Simulation 2. Comparing simulation results for the different cubic EOS for CO2 against SW. (b) Simulation results from [5].

Conclusions

We have demonstrated via numerical simulations, that having the correct thermal properties can significantly influence the outcome of numerical simulations modeling the injection and subsequent flow and storage of the CO_2. In particular, comparing the different classes of cubic EOS against the SW data for CO_2, we can conclude that

- Standard cubic EOS formulations lead to incorrect CO_2 properties near the critical point, and within the super-critical region.
- A generalized cubic EOS gives a better approximation of the CO_2 density and therefore better flow behavior in buoyancy driven systems.

Acknowledgements

Appendix A. Simulation parameters

Table A.3. Fluid and rock properties[3] for Simulation 1

Property	Value
brine density	1182 kg/m^3
brine viscosity	7.185×10^{-4} Pa. s
brine enthalpy	$f(p,T)$
CO_2 density	$f(p,T)$
CO_2 viscosity	$f(p,v)$
CO_2 enthalpy	$f(p,T)$
rock density	2650 kg/m^3
rock heat capacity	750 J/(kg K)
rock thermal conductivity	1.0 W/(m K)

Table A.4. Reservoir properties and rock-fluid parameters for Simulation 1.

Property	Value
permeability	1×10^{-12} m^2
porosity	0.2
residual brine saturation	0.2
residual CO2 saturation	0.05
relative permeability	Brooks-Corey
capillary pressure	Brooks-Corey
entry pressure	1000 Pa
Brooks-Corey parameter λ	2.0

References

[1] Aavatsmark, I. Generalized cubic equation of state. In: EarthDoc, *Fourth EAGE CO₂ Geological Storage Workshop*, www.earthdoc.org/publication, 2014.

[2] Aavatsmark, I., Kometa, B.K., Gasda, S.E. Thermal simulation of CO_2 with generalized cubic equation of state. In: EarthDoc, *ECMORXIV*, www.earthdoc.org/publication, 2014.

[3] Bielinski, A. *Numerical simulation of CO₂ sequestration in geological formations*. Ph.D. thesis, University of Stuttgart, Germany, 2006.

[4] Class, H., *Models for non-isothermal compositional gas-liquid flow and transport in porous media*, Ph.D. thesis, University of Stuttgart, Germany, 2007.

[5] Class, H., Ebigbo, A., Helmig, R., Dahle, H., Nordbotten, J., Celia, M., Audigane, P., Darcis, M., Ennis-King, J., Fan, Y., Flemisch, B., Gasda, S.E., Jin, M., Krug, S., Labregere, D., Naderi Beni, A., Pawar, R., Sbai, A., Thomas, S., Trenty, L., Wei, L. A benchmark study on problems related to CO_2 storage in geologic formations, *Comput. Geosci.* 13 (4) (2009) 409–434.

[6] Class, H., Helmig, R., Bastian, P. Numerical simulation of non-isothermal multiphase multicomponent processes in porous media 1. An efficient solution technique, *Advances in Water Resources* 25 (6) (2002) 533–550.

[7] CMG, Computer Modeling Group, www.engroup.com/software/brochures/GEMFactSheet.pdf, 2006.

[8] Fenghour, A., Wakeman, W., Vesovic,V. The viscosity of carbon dioxide, *J. Phys. Chem. Ref. Data* 27 (1) (1998) 31–44.

---

[3] The symbol *f* is used to denote functions of the given arguments.

[9] Heimsund, B.-O. *Mathematical and numerical methods for reservoir fluid flow simulation,* Ph.D. thesis, University of Bergen, Norway, 2005.

[10] Schlumberger. *Schlumberger Information Systems*, ECLIPSE Technical Description, 2007.

[11] Span, R., Wagner, W. A new equation of state for carbon dioxide covering the fluid region from the tripple-point temperature to 1100 K at pressures up to 800 MPa*, J. Phys. Chem. Ref. Data* 25 (6) (1996) 1509–1596.